

EVALUATION OF RESERVOIR STOOIP AND ROS FROM LABORATORY MEASUREMENTS ON CARBONATES WITH EMPHASIS ON THE ROLE OF PORE LEVEL FLUID DISTRIBUTION AND WETTABILITY

M. Dernaika¹, M. S. Efnik², M. Z. Kalam², M. Al Mansoori², Jorge Gomes², Bruno Stenger² and S. M. Skjæveland³

(1) ResLab L.L.C., Abu Dhabi, (2) ADCO, Abu Dhabi, (3) University of Stavanger, Stavanger

Society of Petrophysicists and Well Log Analysts

Copyright 2009, held jointly by the Society of Petrophysicists and Well Log Analysts (SPWLA) and the submitting authors.

This paper was prepared for presentation at the SPWLA 50th Annual Logging Symposium held in The Woodlands, Texas, United States, June 21-24, 2009.

This interpretation of capillarity and resistivity results shed more light on the strong relationship between pore geometry and Wettability and their role in water-oil displacement studies.

ABSTRACT

Carbonate reservoir core plugs with different reservoir rock types were subject to a laboratory study to determine representative initial water saturations, as well as remaining oil in water flooded regions. Reservoir rock types were selected based on X-ray CT scans, NMR T2 distributions, high pressure mercury injection (MICP), porosity, permeability and Thin Section descriptions. Petrophysical SCAL tests were conducted on the chosen samples using the Porous Plate method at reservoir temperature and net overburden pressure conditions. The results of Primary Drainage (PD), Spontaneous Imbibition (SI) and Forced Imbibition (FI) experiments are presented in this work to capture the capillary pressure (P_c) behavior and the electrical resistivity (RI-Sw) changes all the way to irreducible brine saturation (S_{wi}) for drainage and residual oil saturation (S_{or}) for imbibition. Both S_{wi} and S_{or} results were validated with appropriate logs and sponge core measurements. The impact of both drainage and imbibition laboratory results for the field and hysteresis in RI-Sw measurements were also considered.

Capillary pressure and Resistivity Index data when grouped according to geological lithofacies confirm the distinct RRT characteristics. Interesting capillary pressure behavior has been observed in the spontaneous imbibition cycle which can directly be linked to the pore throat size distribution curves obtained from mercury injection data on corresponding sample ends. The capillarity behavior could be explained on the basis of pore level fluid distribution scenario which was detected from corresponding resistivity measurements.

Integration of the capillary pressure, water saturation and resistivity index results together with the basic Petrophysical data including porosity, permeability, NMR, CT scans, mercury injection and Thin Section images enhances the consistency of the collected data. The value of the well defined laboratory data and its integration to logs is pertinent to a confident reservoir characterization. Despite the reservoir zone of interest being classed as intermediate to oil wet conditions, 'n' values are lower than the previously assumed value of 2, and much lower than that expected for pseudo oil wet conditions. The work presented reduced the uncertainties in the oil in place estimations and allowed a realistic evaluation of the water flooding performance.

INTRODUCTION

Porous Plate

Capillary pressure curves (P_c) and electrical resistivity measurements (Sw-RI) are two most important parameters in formation evaluation. Porous plate technique offers robust and dependable acquisition of water-oil P_c and Sw-RI at reservoir conditions using dead crude oil and simulated formation water (during both primary drainage and imbibition cycles) [Kalam et al]. The importance of the porous plate method in establishing P_c and Sw-RI comes from the fact that connate water and remaining oil in the reservoir occur through the mechanism of immiscible fluid displacement which involves capillary action.

Wettability

Most laboratory measurements of capillary pressure and resistivity index are now being performed at reservoir

temperature using crude oil to restore wettability of the rock sample. Wettability restoration is considered imperative for obtaining a physical behavior representative to the conditions in the reservoir.

One of the most widely used indications for wettability is the spontaneous positive imbibition part in capillary pressure experiments. Figure 1 shows a schematic plot on expected imbibition capillary behavior under different Wettability conditions [Masalmeh]. This behavior can be visualized as no water can spontaneously imbibe back into the sample if the rock surface had been converted to strongly oil wet. The opposite behavior would occur (imbibe a lot of water spontaneously) if the rock remains strongly water wet. The mixed wettability condition capillary behavior would probably be somewhere in between.

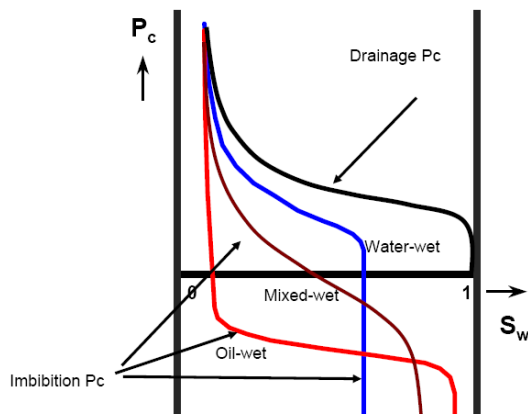


Fig. 1 Expected imbibition curves under different Wettability conditions [Masalmeh]

Log calibration

The electrical resistivity of a fluid-saturated rock is its ability to impede the flow of electric current through that rock. Sw-RI data allow laboratory determination of the saturation exponent ‘n’ which in turn is used to quantify fluid saturations from resistivity logs across the zones of interest in a hydrocarbon bearing formation.

Saturation exponents derived under drainage mode represent the drainage conditions found in the virgin state of most hydrocarbon reservoirs. Such saturation exponents are most appropriate for the calculation of oil in place and reserves. However, if the reservoir is under water flooding, imbibition conditions prevail and hence saturation exponents should be derived in the lab under imbibition mode for accurate determination of remaining oil.

EXPERIMENTAL PROCEDURES, RESULTS & DISCUSSIONS

Sample Selection and Preparation

Forty four reservoir core plug samples were screened to obtain representative rock types present in a carbonate reservoir zone from a producing field in the Middle East. The core plugs were 1.5” in diameter and the sampling strategy for SCAL was based on X-ray CT scanning, Thin Section description, mercury injection measurements and poroperm analysis. The reservoir core samples examined comprised 8 reservoir rock types (RRT) with porosity ranges from 10-33% and permeability ranges from 0.01-6000 mD.

Figure 2 presents the porosity permeability trends for the selected SCAL plugs (20 plugs). This shows the distinct RRT classification in the groupings of samples selected. The selected core samples underwent two-stage hot flush cleaning cycles with various solvent combinations in order to render the samples more water wet. The cleaning procedure was an optimized technique that had been examined in previous studies on similar rocks and verified through restored wettability experiments.

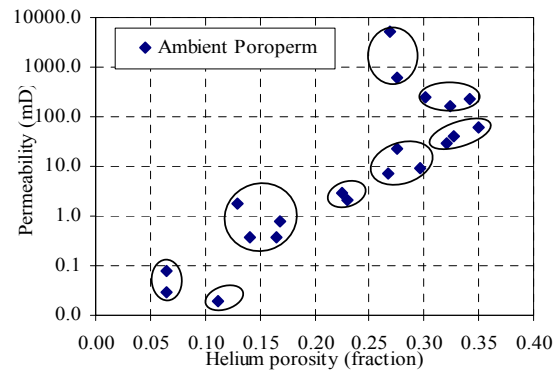


Fig. 2 Poroperm distribution and RRT

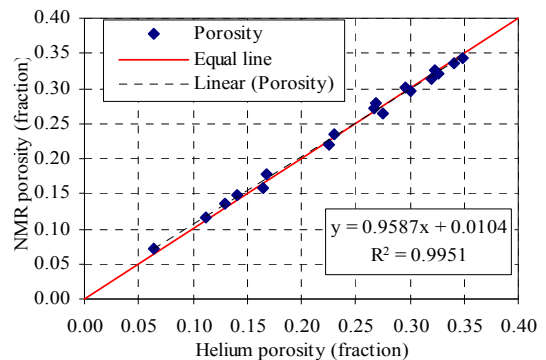


Fig. 3A NMR Vs He Porosity

NMR Analysis

NMR T2 relaxation times were measured on brine-saturated samples using an echo-spacing of 200 micro seconds. The T2 distribution obtained from rocks saturated with a single fluid phase wetting the surface of the pores reflects the pore size distribution of the rocks where pore size is measured as the ratio between its surface area and volume (Kenyon et. al., 1986). It is interesting to note that there is a good correlation (in figure 3B) between permeability and mean T2 values indicating that the shape and position of the T2 distributions for the saturated samples, is dependent on the size and distribution of the main flow channels within the pore space. All samples had NMR porosity values within 1.1 porosity units (p.u.) of the helium porosity (Figure 3A).

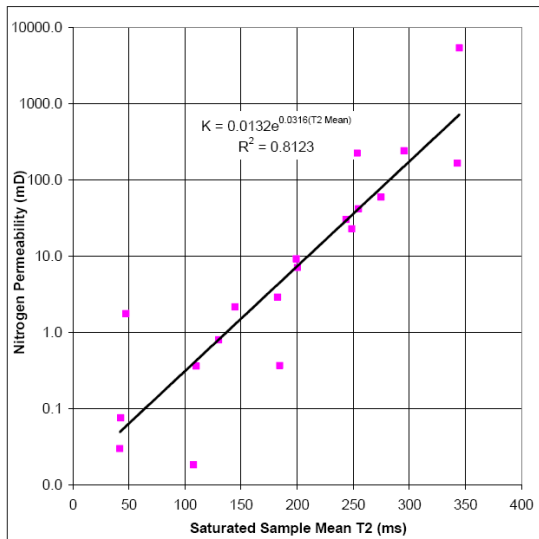


Fig. 3B K_g Vs T_2

Formation Resistivity Factor

Figures 4 and 5 show the evaluated cementation exponents ‘m’ at ambient and reservoir temperatures, respectively. These confirm ‘m’ to increase slightly from 1.95 to 1.98 upon applying a reservoir temperature of 121°C, at the same reservoir overburden pressure. Figure 6 shows a decrease in FF with increasing permeability below approximate value of 10 mD. This behavior is controlled by changes in pore geometry which can also be linked to changes in permeability. However, the fairly constant FF with permeability for the rocks higher than 10mD could be due to similarities in the pore geometry for those rocks despite the large changes in permeability.

Mercury derived capillary pressure curves confirm similarities in pore geometry for the highly permeable samples (RRT 1-4 in figure 7) and at the same time

confirm differences in pore geometry for the samples with permeability lower than 10mD (RRT 5-7 in figure 8).

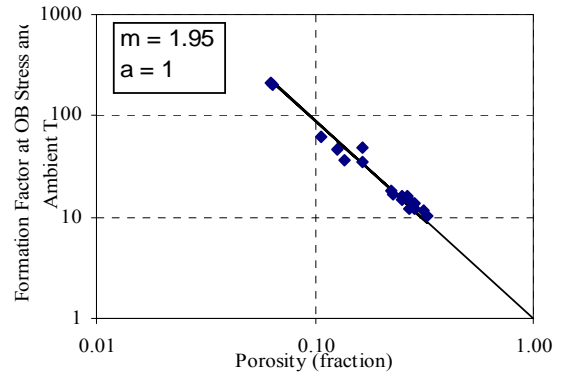


Fig. 4 FF Vs Porosity at OB, Ambient T

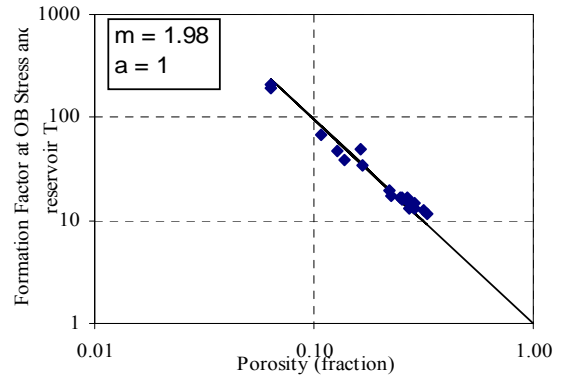


Fig. 5 FF Vs Porosity at OB, High T

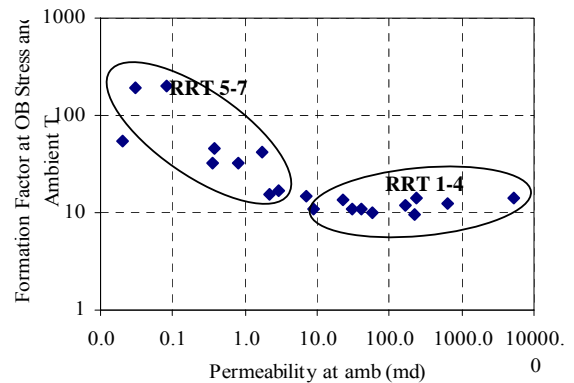


Fig. 6 FF Vs Permeability at Ambient T

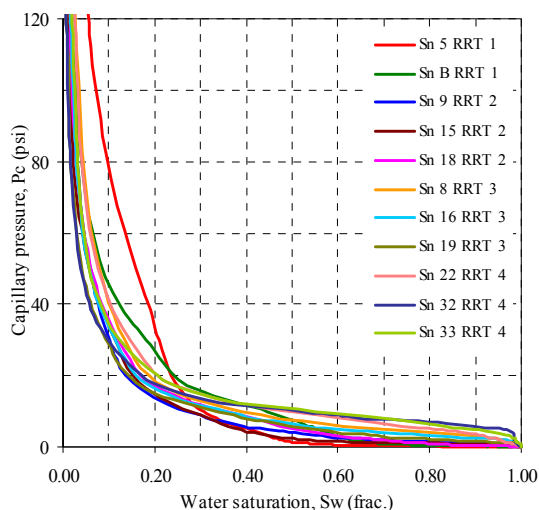


Fig. 7 Hg-derived P_c curves for RRT 1-4

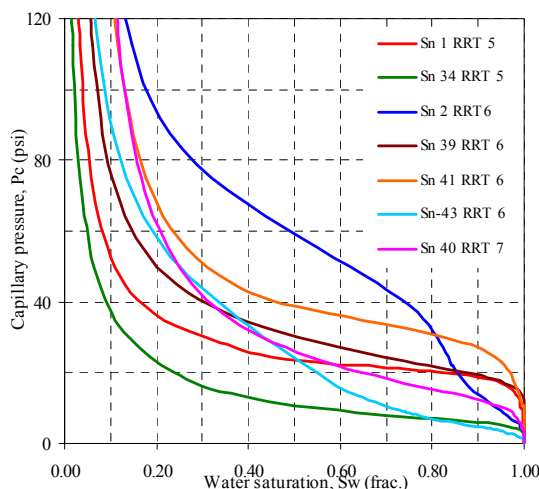


Fig. 8 Hg-derived P_c curves for RRT 5-7

Capillary Pressure and Resistivity Index

Primary Drainage Cycle

Combined capillary pressure curves and resistivity index plots were generated by the ceramic porous plate method [Longeron and Wilson et al]. All measurements were performed under net overburden pressure and reservoir temperature using stock tank oil as the displacing fluid. The core plugs were de-saturated by increasing capillary pressure in steps and recording resistivity and expelled water on a daily basis. Figures 9 and 10 represent initial water saturation versus porosity and versus permeability respectively. The figures show the impact of pore geometry on the evaluated S_{wi} at the end of primary drainage cycle. These two figures confirm the conclusions derived from figures 6, 7 and 8.

Figures 11 and 12 represent typical time steps applied during the equilibrium measurements for the drainage cycle (brine de-saturation), and confirm the long times required for good P_c and Sw-RI data. A full drainage cycle can typically take between 4 to 6 months for many of these carbonate samples. Figures 13 and 14 typify the RI-Sw and P_c data, respectively from such measurements. In figure 13 it is seen that both transient and equilibrium data follow the same trend. Figure 14 also shows a comparison with the water-oil P_c derived from mercury intrusion on the trim of the same sample at no confining stress; the differences can be attributed to the assumed IFT conversions as well as to sample size. Such plots, however, enhance confidence in the measured water-oil drainage P_c data from the porous plate.

Figure 15 presents measured water/oil primary drainage P_c curves on RRT 1-4 plug samples and figure 16 presents the P_c curves obtained on RRT 5-7 plug samples. These curves are generated on the main SCAL plugs using STO-Brine fluid system. These plots confirm the rock type classification presented in figures 7 and 8 and the similarity in results to the mercury derived P_c curves.

When the RI-Sw plots are examined (as in figure 17), 'n' is shown to vary from 1.99 to 1.61. The range in the data is reminiscent of previously examined data from another reservoir zone of the same field [Fleury et al] although the non-linear behavior observed in the previous study in some of the samples were totally absent in the current study. Further, the data set is consistent and repeatable in showing 'n' approaching 2 in most of the prolific rock types (RRT 1 – RRT 5) while the less permeable RRT (6-8) samples show 'n' approximately around 1.6. The significance of this analysis is demonstrated by examining logs in the same well, and in other wells.

Samples from RRT 8 could not undergo primary drainage measurements due to the tight nature of the core plugs (Crude oil could not invade the pores at the highest applied capillary pressure).

Leveret J Function

The impact of using J-function for grouping P_c curves is investigated in figure 18 for all RRT samples. It is evident that the J-plot is not adequate to group the P_c curves for rocks of such carbonate nature. On the contrary, the J-functions show scattered data for RRT 1-4 samples compared to the normal P_c curves for the same samples in figure 19. Moreover, the J-function in figure 18 suggests that the P_c curves of the higher permeability samples (here RRT 1-4) are shifted up and to the right, whereas the normal and actual P_c curves in

figure 19 shows that those curves should be shifted to the left which is indeed the expected and correct behavior. The J function for these RRT's is giving wrong representation of the Pc curves. The wrong behavior is probably due to the simplification (mathematics) of the J function equation,

$$J = \sqrt{\left(\frac{k}{\phi}\right)} \cdot \frac{P_c}{\sigma \cdot \cos \theta}$$

Where

J = Leveret Dimensionless Function.

k = Permeability, mD.

Φ = Porosity, fraction.

P_c = Capillary pressure, psia.

σ = Surface tension, dynes/cm

θ = Contact angle, °

When the permeability value does not wholly represent the pore geometry of the rock sample (as in our case here) then the J function will give unrealistic behavior of the capillary pressure. The reason the J curves of the RRT 1-4 samples were shifted up and to the left in figure 18 was due to the high permeability values of those samples that increased the J function value and gave overestimated figures. Hence, we conclude that the J function should not be solely used for such complex rock types and that - when this function is used for other samples - the curves should be checked carefully with the actual Pc behavior generated on rock samples. It is worth mentioning that several attempts had been made to upgrade the Leveret J function by using modified J function with dimensionless water saturation (El Khatib and Desouky). This modified function was not tried on these samples and therefore was kept for future investigations.

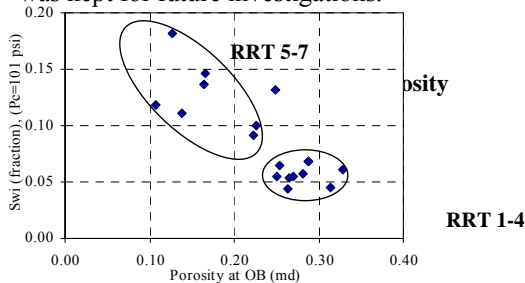


Fig. 9 Swi Vs porosity

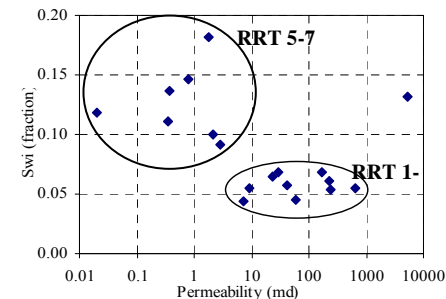


Fig. 10 Swi Vs Permeability

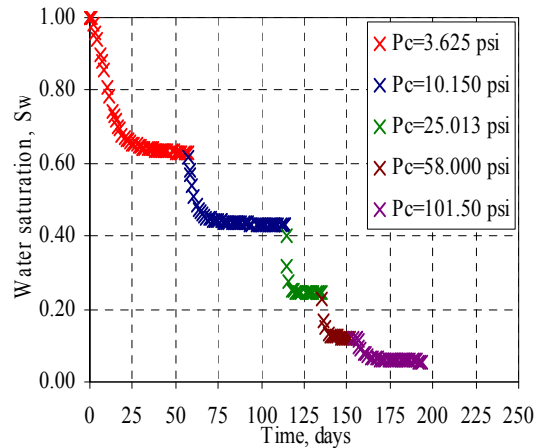


Fig. 11 Sw Vs Time – Plug B

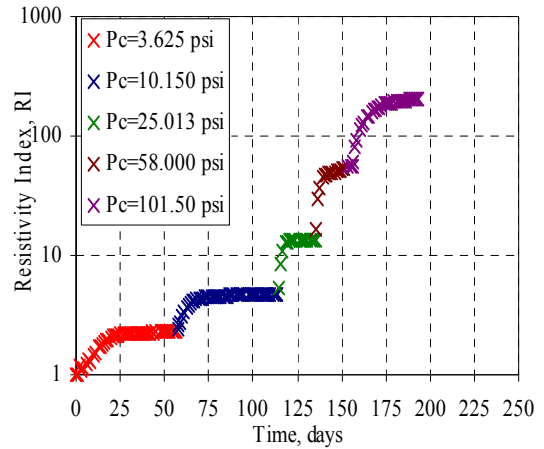


Fig. 12 RI Vs Time – Plug B

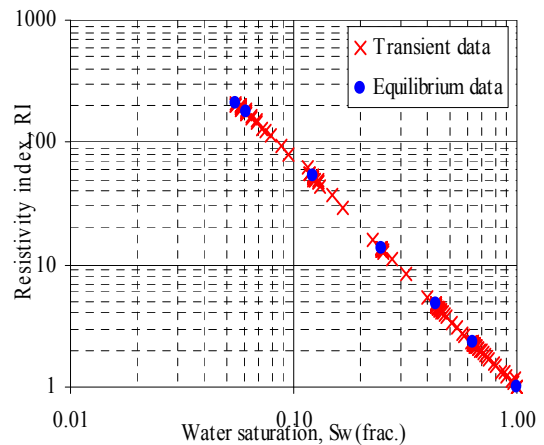


Fig. 13 Transient Data RI Vs Sw – Plug B

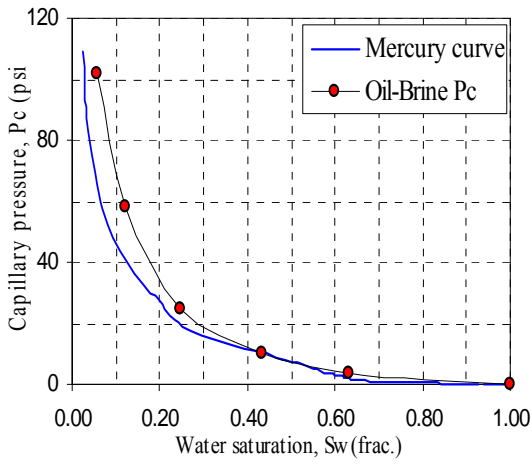


Fig. 14 Capillary Pressure Curves – Plug B

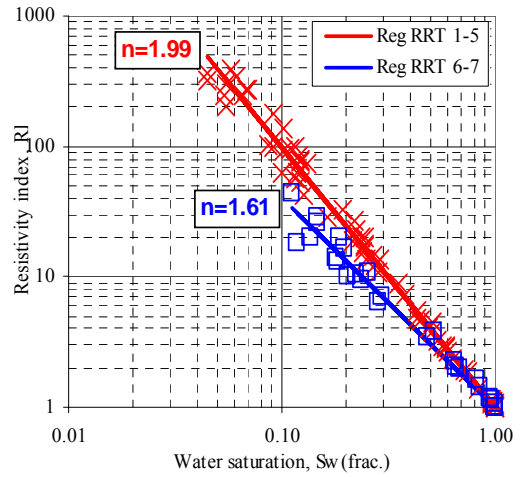


Fig. 17 RI Vs Sw for all Samples

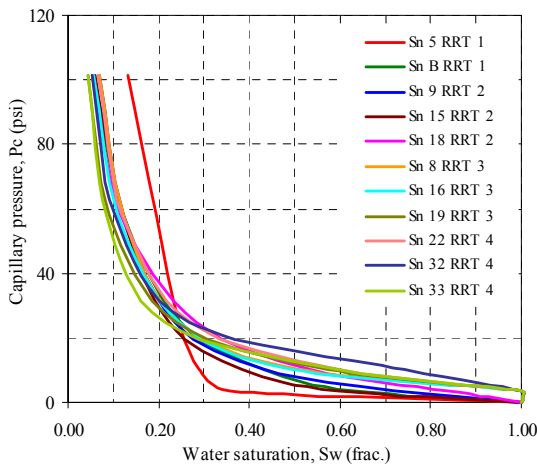


Fig. 15 Pc curves for RRT 1-4 plugs

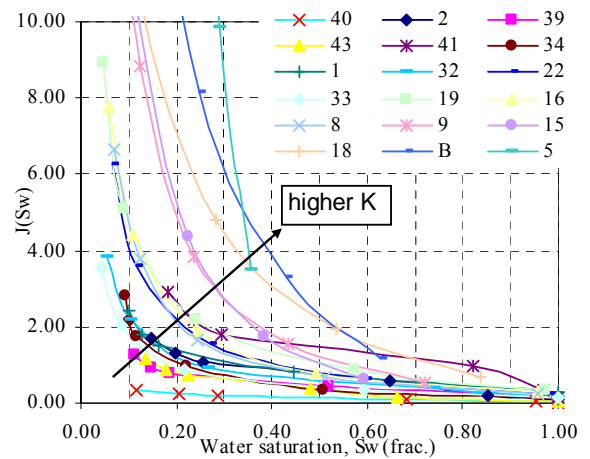


Fig. 18 J-Function Plot – all plugs

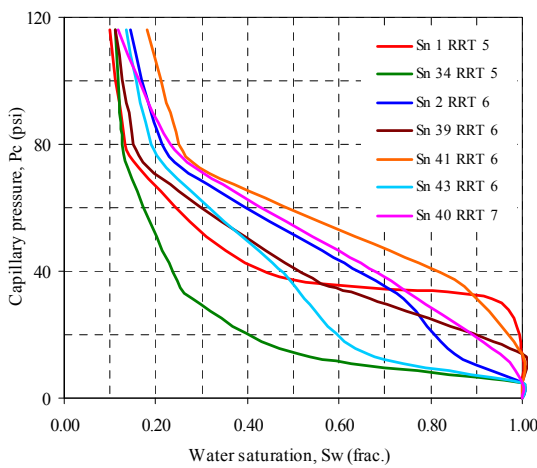


Fig. 16 Pc curves for RRT 5-7 plugs

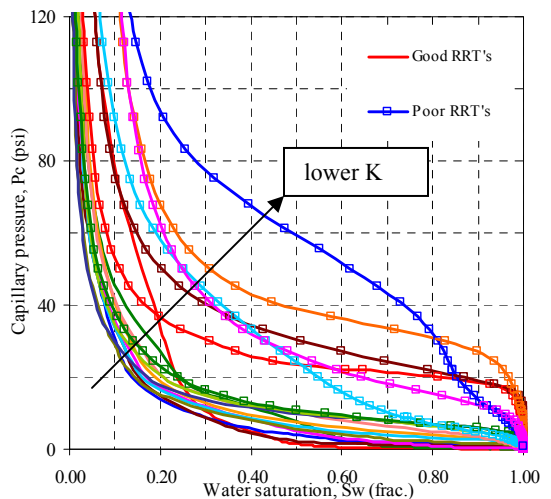


Fig. 19 Pc Plot – all plugs

Spontaneous Imbibition (SI) Cycle

The spontaneous imbibition (SI) measurements were performed as a continuation of the primary drainage cycle at the same experimental conditions. The core plugs were saturated with simulated formation brine (SFB) spontaneously by decreasing the capillary pressure in steps (from max P_c to zero) and recording resistivity and imbibed water on a daily basis. Figures 20 and 21 depict the spontaneous imbibition P_c behavior of RRT 1-4 samples and RRT 5-7 samples respectively. The spontaneous imbibition cycle started after the rocks had been in contact with crude oil at reservoir temperature for about 5 months (end of primary drainage cycle). The SI cycle took about 2 months to complete. This means that the rock samples under study had been in crude oil at reservoir conditions for more than enough to alter (or restore) their wettability towards intermediate or oil wetness. If the rocks are no longer water wet at S_{wi} , this makes us feel that the samples will not encounter much spontaneous imbibition and that this cycle will finish fairly quickly.

RRT 1-4 samples indeed did not show much spontaneous imbibition (figure 20). Actually, some of those samples did not show any spontaneous imbibition at all. However, the low permeability samples (RRT 5-7) showed unexpectedly large water imbibition during capillary pressure reduction except one sample (plug # 43) from RRT 6 (figure 21). This is an interesting behavior which could be linked to the pore geometry of the rock samples as well as to Wettability.

Spontaneous Imbibition and Mercury Injection

In figure 21 (RRT 5-7 samples) it is noticed that plug # 43 is the only sample which did not show any spontaneous imbibition while all the other samples encountered large water imbibition. We first believe this phenomenon can be explained by examining the mercury derived pore throat size distribution (PSD) obtained on corresponding end trims of each individual plug sample. Figures 22 to 27 present comparison plots of the PSD of plug # 43 to the PSD for each plug in the RRT5-7 samples.

It can be clearly seen that sample # 43 has the widest distribution among all the other samples in this group. The other samples have relatively narrow and uniform pore throat size distribution curves. The narrow and uniform PSD of the imbibing samples can be visualized as a bundle of uniform capillary tubes with small radii that are able to raise fluid (water) to high levels. This is the unique pore geometry which governed the spontaneous imbibition behavior in these rock types. The wide and heterogeneous PSD of sample # 43 did not allow the sample to imbibe water spontaneously.

Another interesting observation in figure 21 is the capillary behavior of sample # 1 which can also confirm our argument above. This sample had the largest imbibition in the SI cycle. If we consider its pore size distribution we will see that this sample has got the narrowest and the most uniform PSD among all imbibing samples.

RRT1-4 samples did not imbibe much water in the SI cycle due to the wide and heterogeneous distributions of their pore throats as shown in figure 28.

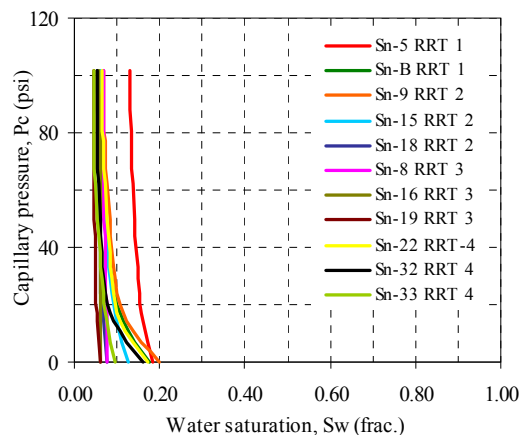


Fig. 20 Spont Imb P_c curves - RRT 1-4

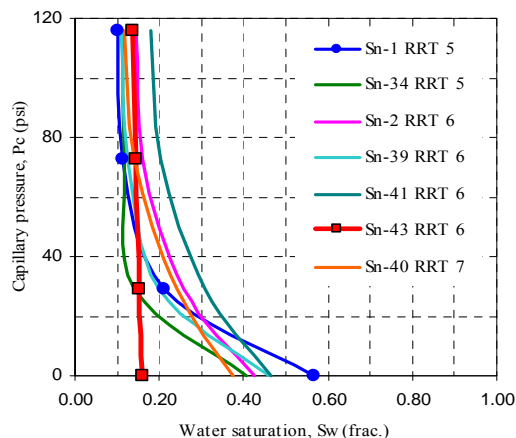


Fig. 21 Spont Imb P_c curves - RRT 5-7

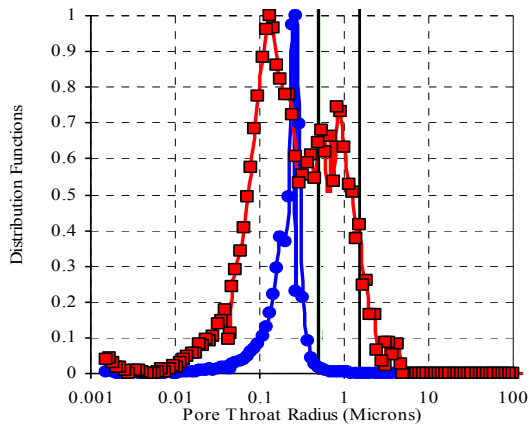


Fig. 22 *Sn-1 RRT 5 Vs Sn 43 RRT 6*

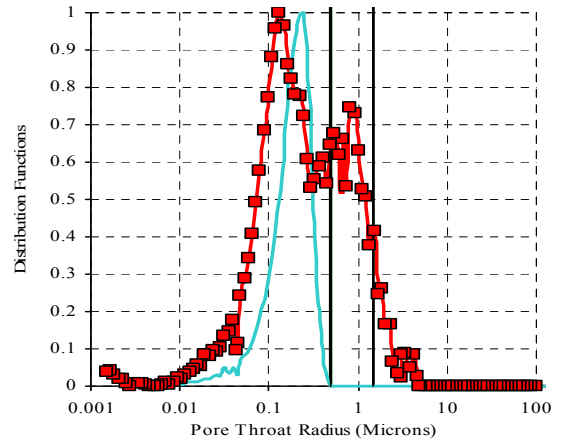


Fig. 25 *Sn-39 RRT 6 Vs Sn-43 RRT 6*

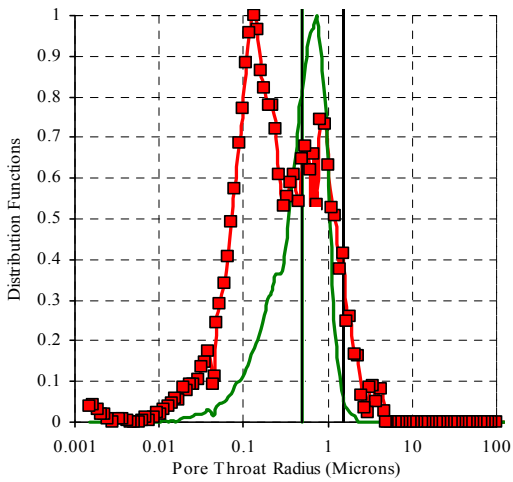


Fig. 23 *Sn-34 RRT 5 VS Sn-43 RRT 6*

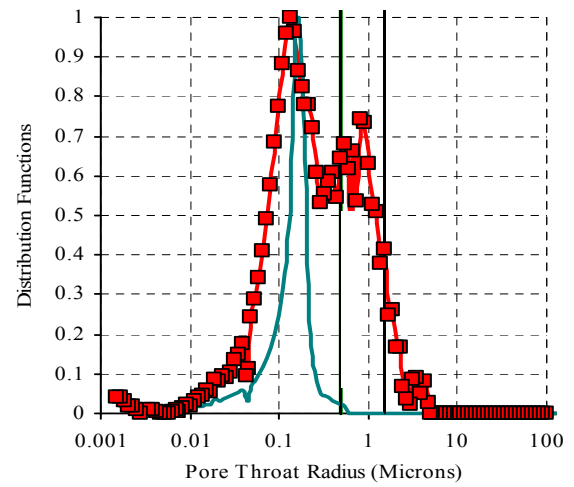


Fig. 26 *Sn-41 RRT 6 Vs Sn-43 RRT 6*

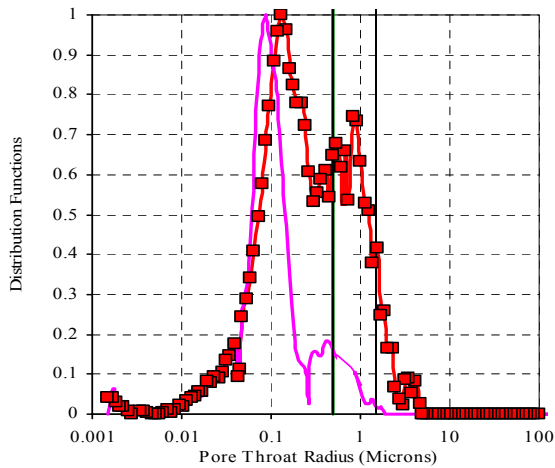


Fig. 24 *Sn-2 RRT 6 Vs Sn 43 RRT 6*

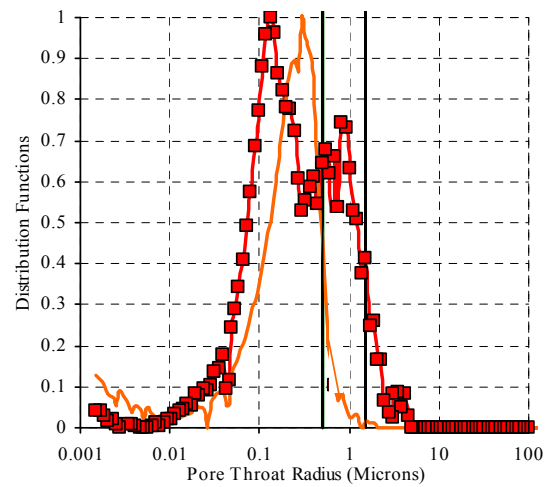


Fig. 27 *Sn 40 RRT 7 Vs Sn 43 RRT 6*

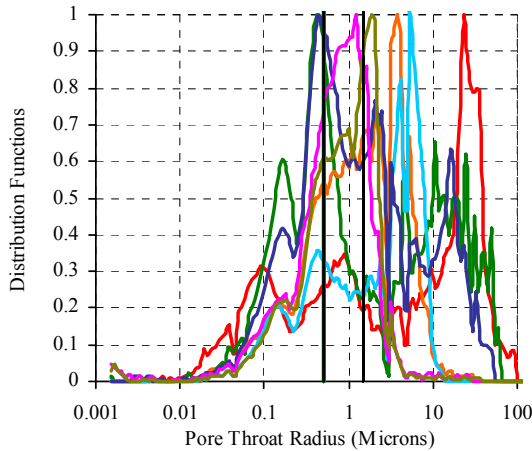


Fig. 28 PSD – RRT 1-4

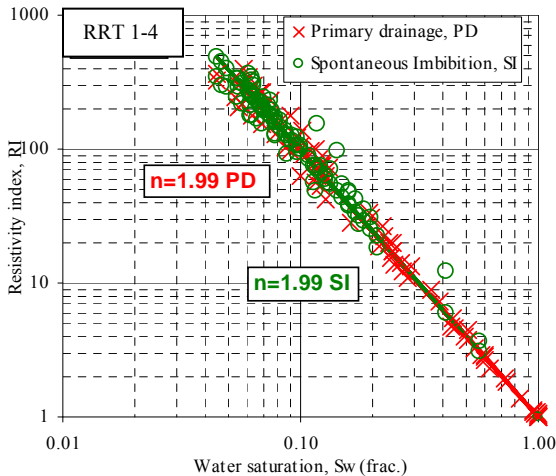


Fig. 29 Composite RI-Sw – RRT 1-4 in SI

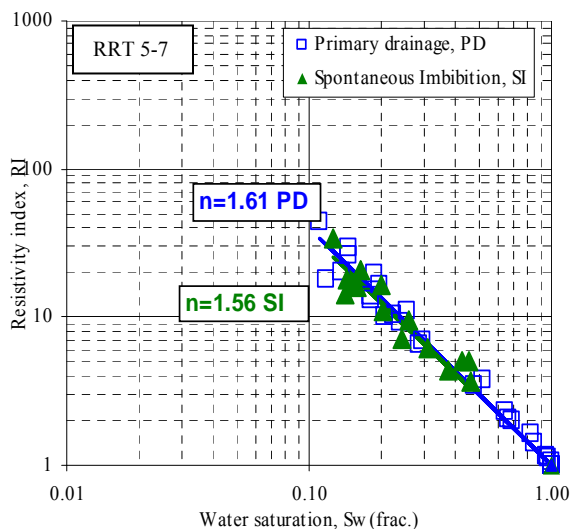
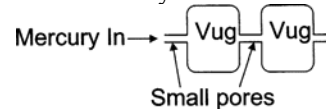


Fig. 30 Composite RI-Sw – RRT 5-7 in SI

Figure 29 shows primary drainage and spontaneous imbibition resistivity index behavior with composite saturation exponent “n” on all samples from RRT1-5. Similarly, figure 30 represent the RI behavior for RRT 6 and 7. The plots confirm the negligible hysteresis effects in the SI cycle.

Comparison of T2 with Mercury Injection Derived Pore Throat Distributions

A comparison of mercury injection pore size distributions and saturated sample T2 distributions can help evaluate if a pore network contains ‘shielded’ pores. RRT 5-7 samples in general, show an excellent match between T2 distributions and mercury injection pore size distributions. Figure 30A represents one sample from this RRT group. This indicates that the pore geometry for these samples approximate the capillary tubes model. On the other hand, the comparison of the two forms of distribution for RRT 1-4 samples show a mismatch. Such an example is shown in Figure 30B. If pores are arranged such that the entrance to a large pore is through a small restriction, the capillary pressure required to fill the large pore will have to be high enough to fill the small entrance pore, as shown schematically:



This may lead to an over estimation of the small pore volume in the mercury injection pore size distributions. This may explain why the observed mercury injection pore throat distribution is centered on smaller pore sizes compared with the T2 distribution derived pore size distribution. The disparity between the two types of pore size distribution may indicate the existence of shielding of large pores by small pores, in addition to experimental artifacts arising from use of different samples in the two tests.

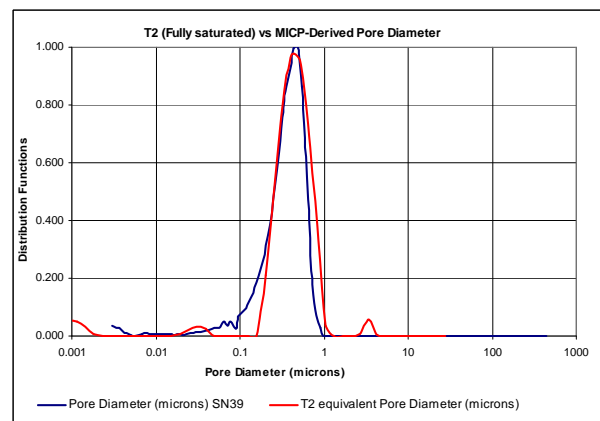


Fig. 30A T2 (Fully saturated) vs MICP-Derived Pore Diameter. Typical behavior for the poor RRT samples.

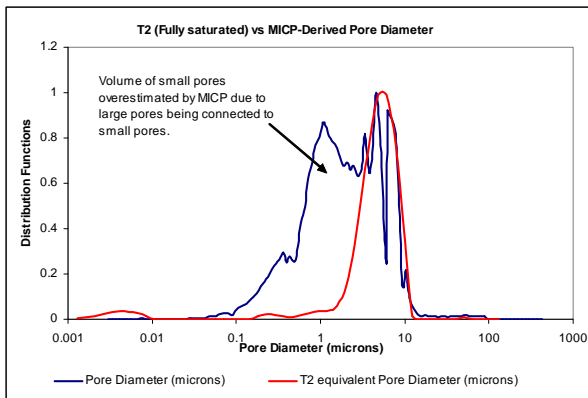


Fig. 30B *T2 (Fully saturated) vs MICP-Derived Pore Diameter. Typical behavior for the good RRT samples.*

The two distinct comparisons between the mercury derived and T2 derived PSD curves (figure 30A and figure 30B) can also emphasize the difference in the spontaneous imbibition behavior observed between the good and the poor RRT samples. The samples which showed high degree of positive imbibition have got uniform pore throat size distribution and their pore networks do not contain shielded pores. This argument may lead us to think of unique pore geometry of the poor RRT samples which governed the fluid distribution during primary drainage and at S_{wi} which in turn allowed spontaneous imbibition to occur. On the other hand, the good RRT samples which are characterized by shielded pores (big pores are surrounded by small pores/restrictions) have shown no or minimum spontaneous imbibition. Again, this unique pore geometry led to unique fluid distribution which did not allow for the spontaneous imbibition to occur.

Of course, it would have been easier to correlate the SI behavior with Wettability but our discussion is going beyond this statement. We are after the reason which made this pore geometry “water wet” and that pore geometry “oil wet”; or in better words: What made the SI behavior in the good RRT samples resemble the oil wet behavior and what made the SI behavior in the poor RRT samples resemble the water wet behavior? This question makes sense here because all the samples were subjected to the same oil/water fluid system at the same experimental conditions. In addition, all the samples almost reached the same S_{wi} value. So, what made that big change in the SI capillary pressure (P_c) behavior? It has to be the difference in the pore geometry which resulted in different fluid distribution (at S_{wi}) and in turn different SI behavior.

The different SI behaviors between the different pore geometry groups may have been caused by one or all of the following combined factors:

Factor 1: PSD from mercury data – Narrow and uniform curves versus wide and heterogeneous curves as discussed earlier. Narrow and uniform pore sizes are associated with high capillary pressures.

Factor 2: The match and mismatch between Hg-derived PSD and NMR derived T2 pore body distributions which revealed the shielding effects of the big pores by the small pores in the good RRT samples. This effect may indicate high aspect ratio (pore body size/throat size) in those samples compared with the poor rock type samples which have uniform pore body and throat distributions. Higher aspect ratio has been shown to yield more pronounced Hains jumps which results in bigger hysteresis (Toledo et al.). Therefore, the minimum SI behavior (bigger hysteresis) observed in the good RRT samples might be due to higher Hains jumps during primary drainage. In contrast, the poor RRT samples imbibed more water (less hysteresis) due to less expected higher jumps in the primary drainage as supported by the excellent match between T2 and Hg PSD curves (low aspect ratio).

Factor 3: The large SI that occurred despite running the tests at reservoir conditions with dead crude oil could be explained by the fluid distribution attained at S_{wi} . Heterogeneous PSD yields heterogeneous Wettability condition caused by different pore sizes present in the rock samples. It was shown (Radke et al) by the aid of the Augmented Laplace equation that larger grains (i.e. larger diameter and hence larger film curvature) exhibit thinner water films due to increases in the disjoining pressure in concave pore geometry. The case would be opposite (i.e. thinner films associated with smaller grain diameter) in convex pore geometry. This argument suggests that water film thickness is a function of grain size - and hence location in the rock sample - even at the same capillary pressure. The thinner the water film is the easier it is to have film rupture which results in surface wettability change from water wet to oil or mixed wet. Therefore, the good RRT samples under investigation, which have large and distinct pores (grains), would exhibit thinner water films than would the poor RRT samples have at the same P_c . This may lead to the conclusion that the larger pores had been converted to oil or mixed wetness faster and more than the smaller pores in the poor RRT samples. In addition, we may conclude that the good RRT samples have experienced heterogeneous wettability whereas the poor RRT samples have experienced homogeneous wettability.

Factor 4: Resistivity Index values attained at S_{wi} for the good RRT samples are much larger than the RI values for the poor RRT samples. This observation is in line with the detected SI behavior and also in agreement with the discussions above.

Forced Imbibition Cycle

Since the reservoir was under water flooding, capillary pressure (Pc) and resistivity index (Sw-RI) measurements were required under imbibition cycle.

The forced imbibition experiment is a key element in evaluating hydrocarbon reservoir performance through the shape of the Pc curve, saturation exponent and residual oil saturation (Sor) [Masalmeh et al, SCA 2003]. The test was a continuation of the spontaneous imbibition cycle and the Pc Sw-RI curves were generated at the same experimental conditions and fluid system by increasing water pressure in constant capillary pressure steps and recording resistivity and imbibed water on a daily basis.

Figures 31 and 32 show the impact of porosity and permeability respectively on the evaluated Sor at the end of forced imbibition cycle. Figure 33 shows the effect of Swi on Sor. All the three plots suggest that there is clear dependence of Sor on poroperm data and Swi between the good and the poor RRT samples. As compared to sponge core data measured on similar core in 2001 and 2008, the good quality rocks RRT1-RRT4 indicated (from sponge data) low Sor (3-5%), whereas, the poor quality rocks RRT5-RRT7 showed relatively high Sor (15-20%) from the same sponge cores. This sponge core result is in line with our observation from SCAL, which gives us more confidence in the acquired measurements.

Figures 34 and 35 represent typical time steps applied during the equilibrium measurements for the forced imbibition (brine saturation), and confirm the long times required for good Pc and Sw-RI data. In these figures the stability criteria for the FI cycle was no resistivity and Sw change for three days. Figure 36 presents the real time transient non-equilibrium RI data for drainage, spontaneous imbibition and forced imbibition on one plug sample (sample # B). Figures 37 and 38 typify the equilibrium Pc and Sw-RI data, respectively from such measurements.

Figure 39 shows the Pc curves on RRT1-4 samples from primary drainage, spontaneous imbibition and forced imbibition cycles. Similarly, the Pc curves are depicted for the RRT5-7 in figure 40.

RRT1-4 samples all showed good agreement in the Pc behavior down to Sor. In figure 40 it is noticed that RRT 5 samples have lower Sor than RRT 6 and 7.

Figures 41 and 42 represent composite Sw-RI plots from all capillary pressure cycles on RRT1-5 and RRT6-7 respectively.

The RI behavior in the FI cycle shows little hesterises in the saturation exponent “n”. The increase in “n” in

RRT 1-5 is from 1.99 to 2.28 while in the RRT 6-7 the increase in “n” is from 1.56 to 1.82.

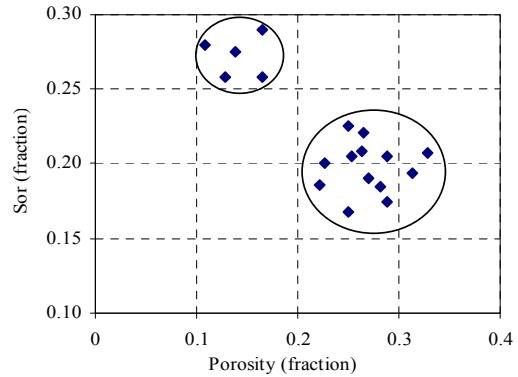


Fig. 31 Sor Vs Porosity

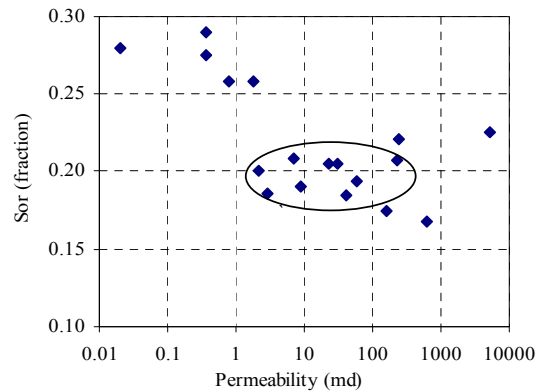


Fig. 32 Sor Vs Permeability

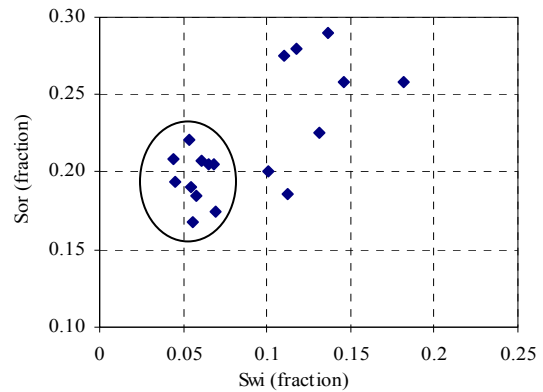


Fig. 33 Sor Vs Swi

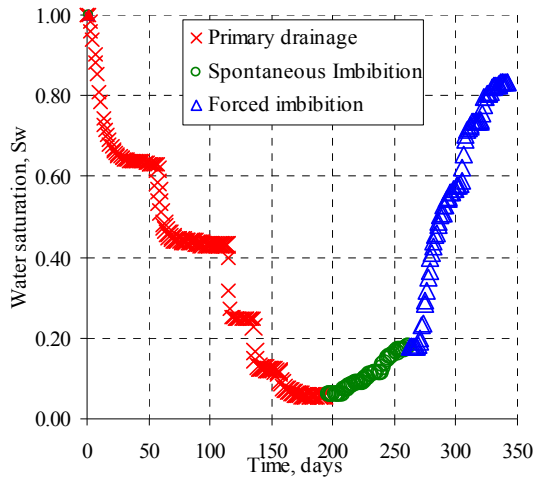


Fig. 34 Water saturation Vs Time Sn-B

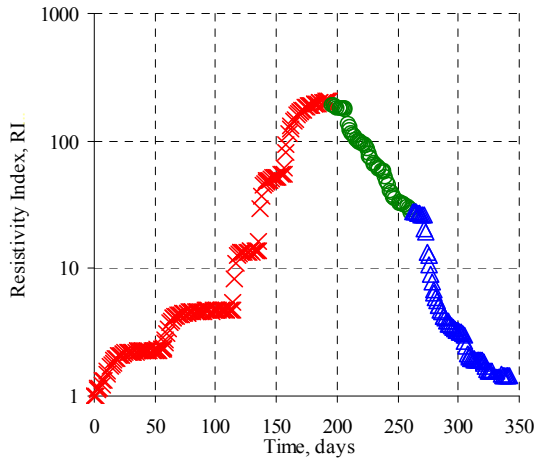


Fig. 35 Resistivity index Vs Time Sn-B

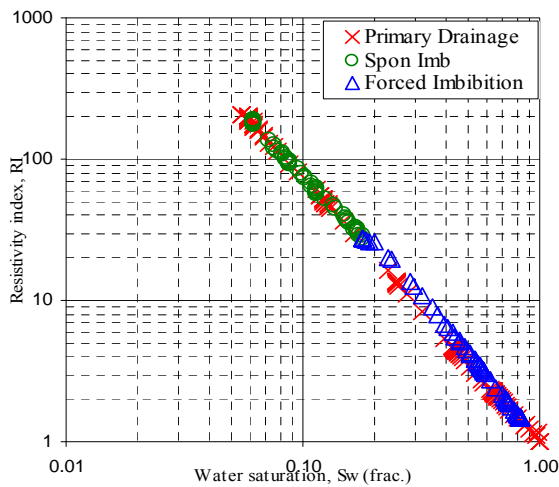


Fig. 36 Resistivity index Vs Sw (transient data)

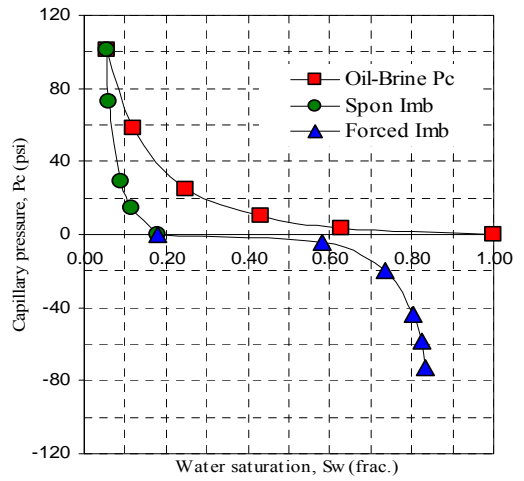


Fig. 37 Pc Vs Sw (equilibrium data) Sn-B

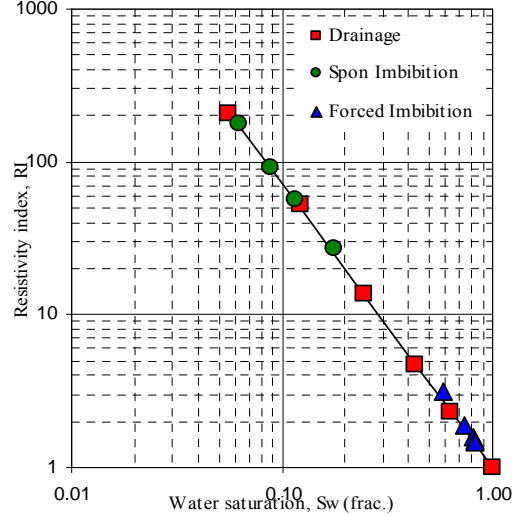


Fig. 38 RI Vs Sw (equilibrium data) Sn-B

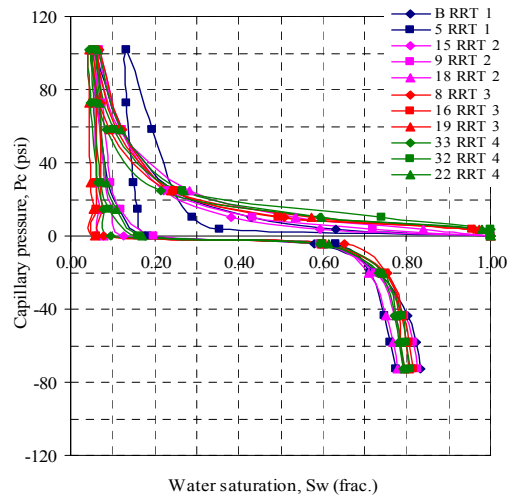


Fig. 39 Pc Vs Sw on RRT 1-4

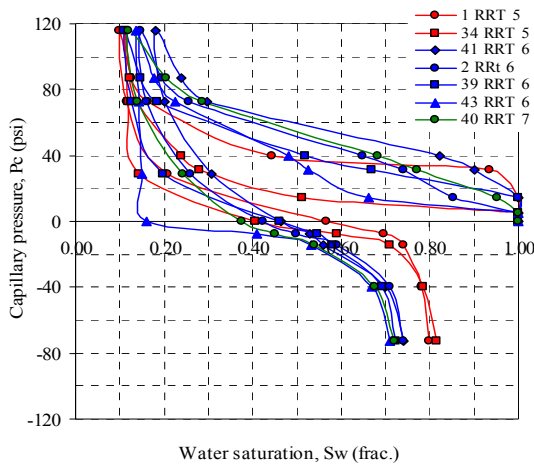


Fig. 40 P_c Vs S_w on RRT 5-7

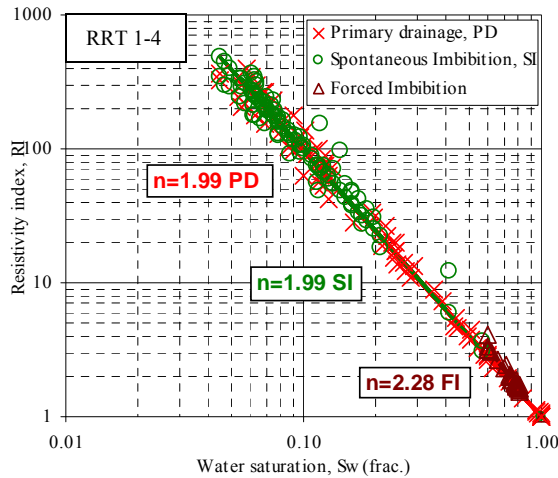


Fig. 41 Composite RI-Sw – RRT 1-5 in FI

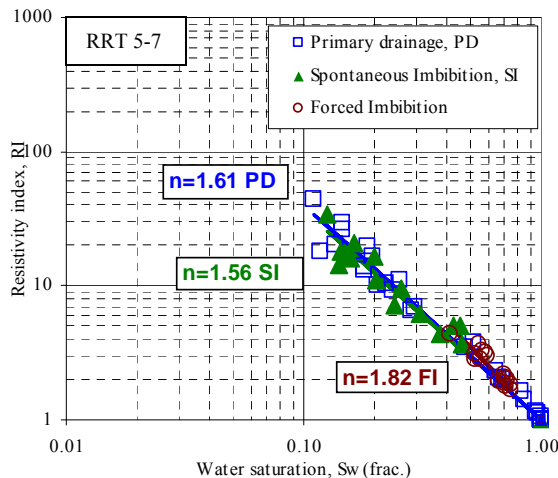


Fig. 42 Composite RI Vs Sw - RRT 6-7 in FI

LOG CALIBRATIONS

Primary drainage

The new SCAL results in drainage are used to calibrate the log response in two wells, one with oil base mud to capture the S_{wi} as accurately as possible (figure 43) and the other one from the study well where the SCAL plugs are taken (figure 44). The new results are compared with the old water saturation calculation using previous data where saturation and cementation exponents were derived mathematically using linear regression analysis. The old parameters ($m=2.15$ and $n=1.78$) are compared with the new parameters using two ranges: an average range where $m=1.95$ and $n=1.99$ representing the two dominant rock types (RRT4 & RRT5) containing most of STOOIP and another where $m=1.95$ and $n=1.60$ for the poor quality rock types. New SCAL data matches closely to that derived from oil base mud (filled dots), and hence more dependable.

Imbibition

The new SCAL data in imbibition is used to calibrate the log response in the study well to capture the S_{or} as accurately as possible (figure 45). Various values of 'm' & 'n', representing different water saturation ranges, have been used to reflect the changes of water saturations due to these new results.

CONCLUSIONS & RECOMMENDATIONS

Porous plate at reservoir temperature and reservoir overburden pressure is indeed a dependable tool for water-oil P_c and RI-Sw measurements during primary drainage, spontaneous imbibition and forced imbibition cycles of carbonate reservoir cores. Interesting observations of RRT dependency on RI-Sw behavior is confirmed in the primary drainage, and shows that 'n' can be as low as 1.60 in tight carbonate samples. The impact on the calibrated logs is significant as a lower 'n' value means a higher amount of remaining oil and STOOIP.

Non-linear RI-Sw behavior in drainage is not observed despite presence of local heterogeneity such as vugs and rudists.

Large hysteresis between drainage and imbibition RI modes were absent in the porous plate tests.

Large spontaneous imbibition was clearly seen in the samples having uniform pore throat size distribution despite long aging time with crude oil at reservoir temperature (121°C). This behavior in capillarity was directly linked pore geometry.

J-function should be used carefully with carbonate rocks. Misleading behavior may be a result of unrepresentative high permeability values.

Measurements like FF, Swi and Sor should not always be linked to permeability and porosity values. Capillary pressure behavior and pore throat size distribution curves are more representative of the pore geometry and hence should be employed to assist in understanding such parameters.

NMR derived porosity is an excellent tool to capture representative carbonate porosities, and needs to be considered as an essential SCAL measurement tool where core matrix preservation is required prior to various displacement tests.

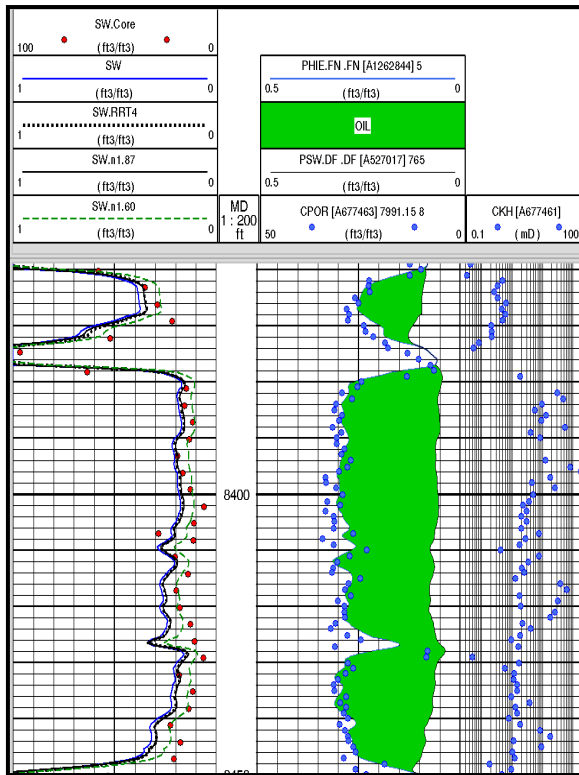


Fig. 43 Comparison of calculated Sw from resistivity log using measured resistivity data with Sw from cores taken with oil base mud.

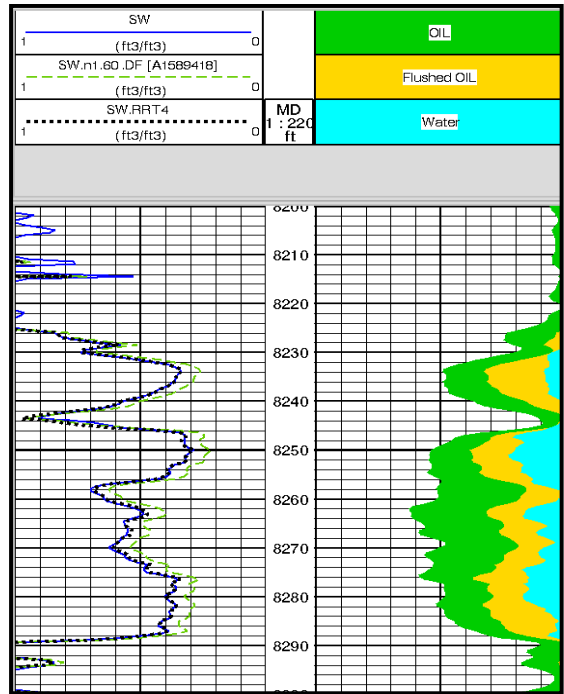


Fig. 44 Study Well

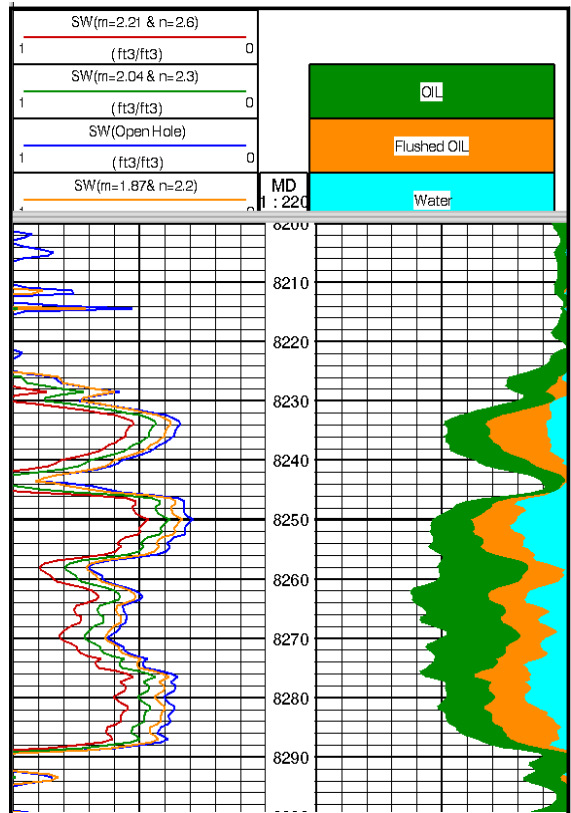


Fig. 45 Comparison of calculated Sw using different 'm' & 'n' values measured during the imbibitions cycles.

ACKNOWLEDGEMENTS

The authors acknowledge ADNOC and ADCO Management for permission to share the contents of this completed study.

REFERENCES

- D.G. Longeron, M.J. Arquad, and L. Bouvier, "Resistivity Index And Capillary Pressure Measurements Under Reservoir Conditions". SPE 19589, San Antonio 1989.
- O.B. Wilson, B.G. Tjetland and A. Skauge, "Porous Plate Influence On Effective Drainage Rates In Capillary Pressure Experiments" SCA 2001, Edinburgh.
- M Fleury, M. S. Efnik and M .Z. Kalam, "Evaluation Of Water saturation From Resistivity In A Carbonate Field", SCA 2004 – 22, Abu Dhabi.
- M Z Kalam et al, "Importance Of Porous Plate Measurements On Carbonates At Pseudo Reservoir Conditions", SCA 2006, Trondheim.
- S. Masalmeh, "Impact of Wettability and Capillary Forces on Water Flood Performance in Heterogeneous Carbonate Reservoirs", Power Point Presentation, Abu Dhabi
- Toledo at el, "Pore-Space Statistics and Capillary Pressure Curves From Volume-Controlled Porosimetry, SPEFE (March 1994) 46-54.
- Radke at el, "A Pore-Level Scenario for the Development of Mixed Wettability in Oil Reservoirs", SPE 24880, 1992
- Kenyon W E, Day P I, Stratley C and Willemsen J F, "Three-part Study of NMR Longitudinal Relaxation Properties of Water Saturated Sandstones", SPE Formation Evaluation, Sept 1986.
- El Khatib, Noaman, "Development of a modified capillary pressure J-Function", SPE 29890, 1995
- Desouky, S.E.D.M, "A new method for normalization of capillary pressure curves", Oil & Gas Science and Technology, Rev. IFP, Vol 58 (2003), No. 5, pp. 551-556